energies

MDPI

Article

Citrus Waste Transformation into Functional Porous Carbon Biochar for Energy Conversion and Storage: Carbonization and Processing Opportunities for Sustainable and Cost-Effective Raw Materials

Rafał Twaróg and Kinga Pielichowska *

Department of Glass Technology and Amorphous Coatings, Faculty of Materials Science and Ceramics, AGH University of Krakow, Al. Mickiewicza 30, 30-059 Krakow, Poland; rtwarog@agh.edu.pl
* Correspondence: kingapie@agh.edu.pl

Abstract

The global production of lemons and limes amounts to approximately 16 million tonnes annually, making these fruits among the most significant contributors to global citrus production. The objective of this study was to investigate the potential conversion of citrus waste derived from lemons into functional porous carbon biochar. The results of thermal analysis of the obtained materials provided valuable insights into the carbonization mechanism of the examined raw materials, which offers a sustainable alternative to conventional carbon sources. The physicochemical and thermal properties of the resulting carbon materials were characterized through analysis of phase transformations of carbonates, structural and elemental composition changes resulting from the preceding treatment process, and electrical conductivity. Research demonstrated that the carbonization of the material must be preceded by an oxidation stage, enabling effective reinforcement of the carbon structure. The oxidation process also directly impacts the reduction of other elemental species. Fourier-transform infrared (FTIR) spectroscopy revealed the presence of functional groups that vary in position and intensity depending on the selected process parameters. It was demonstrated that optimal processing conditions encompass preliminary oxidation of the material at 140 °C, followed by carbonization at 700 °C.

Keywords: lemon biomass; carbonization; energy conversion; phase change materials; porous carbon materials

Check for updates

Academic Editor: Fernando Rubiera González

Received: 24 November 2025
Revised: 30 December 2025
Accepted: 7 January 2026
Published: 10 January 2026

Copyright: © 2026 by the authors. Licensee MDPI, Basel, Switzerland. This article is an open access article distributed under the terms and conditions of the Creative Commons Attribution (CC BY) license.

1. Introduction

The escalating global demand for sustainable materials has intensified research into biomass-derived porous carbon biochars, which could be alternatives to the conventional raw materials currently in use. Among the various approaches to waste valorization, the conversion of agricultural and food processing residues into high-value carbon materials has emerged as a particularly promising strategy that addresses both waste management concerns and the development of advanced functional materials. Global production of lemons and limes amounts to approximately 16 million tons annually, of which an estimated 20% by weight consists of peel and other processing waste, representing a potential for the processing of millions of tons of biomass annually [1–3]. This waste stream consists primarily of peels, pulp, seeds, and pomace, which are currently underutilized despite containing significant amounts of bioactive compounds including phenolic compounds,

carotenoids, vitamins, essential oils, and fibrous materials. Lemon biomass possesses several characteristics that may provide advantages over previously studied biomass sources for the development of carbon aerogels. The high pectin content in lemon peels can serve as a natural binding agent during the hydrothermal conversion process, potentially reducing the need for external binders and improving the structural integrity of the resulting aerogels/foams. Additionally, the presence of limonene and other terpenes in lemon essential oils may influence pore formation dynamics during carbonization, potentially leading to enhanced surface area and porosity characteristics [4–10]. The thermal stability and chemical resistance properties of lemon-derived carbon materials are expected to be superior due to the naturally occurring antioxidant compounds present in the biomass [11,12].

Recent advances in the utilization of lemon biomass have demonstrated the exceptional potential of citrus materials to produce high-performance carbon foams/biochars and aerogels. The conversion of lemon peel waste into functional carbon materials has been achieved through multiple processing pathways, each offering distinct advantages and producing materials with specific characteristics [1,13,14]. One of the most popular processing methods is hydrothermal carbonization. This approach has proven particularly effective for the processing of lemon biomass, operating at moderate temperatures (180–250 °C) under autogenous pressure in a sealed reactor for several hours. This process enables the direct conversion of wet biomass without pre-drying, utilizing water as both solvent and reaction medium breaking down lignocellulosic structures through hydrolysis and dehydration reactions. The method produces hydrochars with an enhanced carbon content (up to 60% dry basis), improved thermal stability, and preserved hierarchical porous structures that are ideal for creating functional carbon biochars. After hydrothermal treatment, the materials are typically subjected to freeze-drying to maintain their three-dimensional structure and create the desired foam-like morphology with low density and high porosity. Sol–gel processing combined with freeze-drying represents another interesting approach that has yielded good results for lemon-based materials [2,9,15–17]. Research by Nie et al. [18] demonstrated the successful synthesis of green composite aerogels based on citrus peel, chitosan, and bentonite through a simple sol-gel and freeze-drying process. These aerogels achieved good Cu (II) adsorption capacities of 861.58 mg/g, substantially exceeding the performance of many conventional adsorbents. Pyrolysis-based approaches constitute the most extensively studied pathway for biomass-to-carbon conversion, with temperature regimes carefully optimized based on desired product characteristics. Slow pyrolysis operates at temperatures between 300–600 °C with heating rates of 5–10 °C/min and extended residence times of 30 min to several hours, maximizing biochar yield while promoting the development of stable carbon structures. Fast pyrolysis employs higher temperatures (450–900 °C) with rapid heating rates exceeding 100 °C/min and short vapor residence times (<2 s), favoring bio-oil production over solid carbon products. Flash pyrolysis represents the most extreme conditions, utilizing temperatures up to 900 °C with heating rates of approximately 1000 °C/s, achieving complete volatilization in less than one second [19–22].

Although the topic of biomass conversion to carbon materials has been widely described in the literature, there is a noticeable lack of basic research on the use of lemons specifically. Interesting examples of scientific work include those on functional absorbent materials. For example, Weldekidan et al. [23] carbonized lemon peel at 400 °C and then chemically activated it with KOH at 850 °C to produce hierarchical porous activated carbon. The resulting material has a very high specific surface area (up to 2821 m^2/g) and micropore volume (0.70 cm^3/g), making it effective for CO_2 adsorption applications. However, the authors emphasize the applicative properties of the resulting material over investigating the underlying mechanisms governing carbonization [23,24]. One of the most promising applications of carbonates derived from lemon biomass may be thermal energy storage

(TES) materials [25]. Despite significant progress in the processing of lemon biomass, several research gaps remain that warrant systematic investigation. This work aims to present the thermal characteristics related to the possibility of carrying out a simple carbonization process directly from lemon waste taking into account the preliminary oxidation process (Figure 1). The low-temperature pre-oxidation (below 200 °C) enables the production of carbon biochar with optimized thermal conductivity and porosity. The direct influence of preliminary oxidation on the increase in surface conductivity and pore distribution of the obtained porous biochars has been verified. Compared to other popular methods, such as hydrothermal or sol–gel, this approach can be significantly more economical and environmentally friendly (e.g., without the need to use acids or hydroxides, and overall reduction in time and energy consumption). Life cycle assessments demonstrate biomass-derived activated carbons produce 72–80% lower global warming potential than coal-based counterparts, with pre-oxidation further reducing operational energy by diminishing the chemical activation temperature requirement and improving surface reactivity [26].

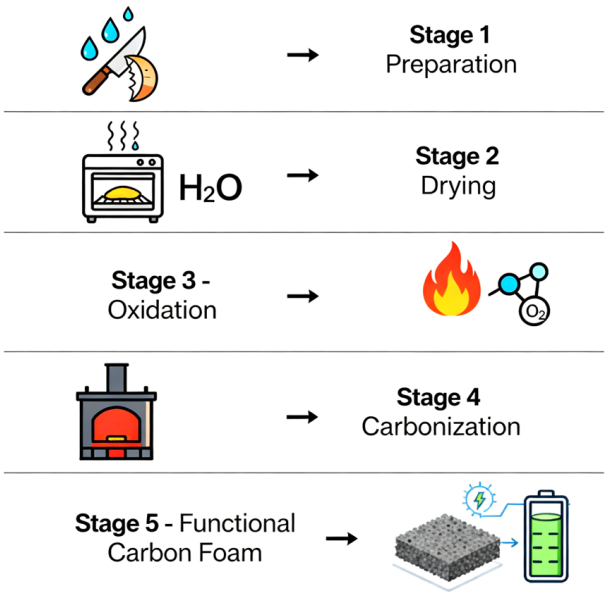


Figure 1. Research work diagram. Stage 1: Preliminary investigation (thermal properties of all lemon anatomical parts); Stage 2: Drying—process simulation and determination of moisture content using TG and DSC techniques; Stage 3: Pre-oxidation study (120–200 °C, 3 min) → morphology, FTIR; Stage 4: Carbonization study (600–800 °C under N_2 atmosphere) → sheet resistance, TG; Stage 5: Characterization of the resulting porous biochar—DSC, morphology, elemental analysis, surface resistance. Source: Perplexity AI, adapted and modified by the author.

2. Materials and Methods

2.1. Materials Preparations

The starting materials examined were lemons commercially available on the market. They were rinsed in distilled water for a period of 2 min. The portion of lemons was cut in half and juiced to reflect the most common use of this raw material in the food industry. The biomass was peeled and crushed into smaller irregular fractions using an automatic blender. The batch size for each experiment was approximately 40 g, corresponding to the average homogenized residue from 3 lemons. Samples prior to analysis were stored in a refrigerator (temperature 4 °C, in air).The biomass was divided into four parts: albedo, yellow peel, the internal part of lemons after juicing without peels—designated in the subsequent text as pulp—and whole fragments from lemons after juicing (whole lemon). Individual sample groups were subjected to comprehensive thermal analysis to determine

the thermal stability of respective lemon parts in both inert atmosphere (nitrogen) and oxidizing atmosphere (air).

2.2. Methods

Thermal analysis methods provided direct verified optimization of individual stages in the functional porous biochar fabrication process. thermogravimetric analysis (TG) was performed using a TGA550 Discovery thermal analyzer (TA Instruments, New Castle, DE, USA). Lemon biomass samples from each experimental section were examined in the temperature range from 40 °C to 950 °C at a heating rate of 10 °C/min under nitrogen atmosphere with a flow rate of 50 mL/min, and in the range of 40 °C to 600 °C in air. The gases used had a purity level > 99.99%.

Fourier transform infrared spectroscopy with attenuated total reflectance (FTIR-ATR) was used to assess structural changes that occur during oxidation of lemon biomass at different temperatures. Measurements were conducted using a Nicolet Apex Thermo Scientific (Waltham, MA, USA) spectrometer equipped with a diamond ATR accessory. All spectra were recorded in the range of 4000–400 cm^{-1} with a spectral resolution of 4 cm^{-1} and 128 scans per spectrum. Data processing was performed using OMNIC Spectra software (TQ Analyst™ software, version 8.0).

The thermal properties of lemon biomass and carbonized materials oxidized at various temperatures were investigated using a differential scanning calorimeter (DSC 1, Mettler Toledo, Greifensee, Switzerland). Approximately 5 mg of each material was placed in a perforated aluminum crucible and analyzed in the instrument. The apparatus was controlled and results were processed using STARe Thermal Analysis Software (V16.40). Materials were heated, cooled, and reheated under nitrogen atmosphere in the temperature range from 0 °C to 500 °C at heating and cooling rates of 10 °C/min.

Microscopic observations of the resulting porous biochar were conducted using an ultra-high-resolution field emission scanning electron microscope (FE-SEM) equipped with a Schottky emitter—NOVA NANO SEM 200 (FEI EUROPE COMPANY. Eindhoven, The Netherlands)—integrated with an energy-dispersive X-ray spectroscopy (EDS) (EDAX, Pleasanton, CA, USA) analyzer. Acquisition time: 10 s, accelerating voltage: 10 kV. The samples were mounted in sample holders using carbon tape. Additionally, to determine compositional changes between individual materials, energy-dispersive X-ray spectroscopy (EDS) analysis was performed, enabling identification and quantification of constituent elements.

The sheet resistance of carbonized samples was determined using an Ossila Four-Point Probe apparatus. The four-point probe method was applied by applying a constant current between the outer probes and measuring the voltage between the inner probes. The system operated within a current range of 1 µA–200 mA, allowing measurement of sheet resistance from 100 mΩ/sq to 10 MΩ/sq.

3. Results and Discussion

3.1. The Conceptual Aim of Optimizing the Carbonization Process of Lemon Biomass

The optimization of the carbonization process consisted of multiple stages (Figure 1). Initially, based on the results obtained regarding the overall thermal properties of lemon-derived biomass, the appropriate drying conditions (time and temperature) were determined. This step was crucial for the properties of the resulting porous biochars, as controlled moisture removal directly influences the preservation of pore structure and surface characteristics during carbonization. Excessive temperature or prolonged drying time leads to premature thermal degradation of valuable biocomponents (hemicellulose, cellulose) and alters the chemical reactivity of the biomass, which can decrease the efficiency

of subsequent processing steps. Controlled drying conditions allow moisture content to be reduced to the optimal level while minimizing energy consumption, a factor critical to both energy efficiency and economic viability.

The dried whole-lemon samples served as feedstock for the next stage—the oxidation process. Optimizing this step is critically important for two main reasons. First, controlled oxidation introduces oxygen-containing functional groups that promote structural crosslinking and form stable covalent bonds within the biomass matrix, preventing melting and uncontrolled restructuring of the carbon framework during high-temperature carbonization. Second, this process significantly reduces carbon loss during pyrolysis while increasing carbon yield by up to 15–25%, resulting in improved structural characteristics of porous biochars, including improved thermal stability, appropriate porosity, and improved mechanical properties of the final material [27–29].

The final stage involved selecting the appropriate carbonization temperature, which directly controls the development of pore structure, the degree of graphitization, and the physicochemical properties of the final material. The process temperature determines the balance between micropore and mesopore formation by regulating the dehydration, hydrolysis, and aromatization reactions of lignocellulose, thus influencing the adsorption capacity as well as the thermal and electrical conductivities of the biochars. Moreover, maintaining a controlled carbonization temperature prevents excessive pore-structure collapse at excessively high temperatures or insufficient carbonization at lower temperatures, enabling precise tailoring of the material's functional properties for applications in energy storage, chemical absorption, and composite materials. The description of the names of the samples created is included in Table 1.

Table 1. Description of the naming of the samples created.

Sample Naming	Description
Lemon	Lemon biomass
Lemon 120 °C ox	Lemon biomass pre-oxidized at 120 °C
Lemon 140 °C ox	Lemon biomass pre-oxidized at 140 °C
Lemon 150 °C ox	Lemon biomass pre-oxidized at 150 °C
Lemon 160 °C ox	Lemon biomass pre-oxidized at 160 °C
Lemon 175 °C ox	Lemon biomass pre-oxidized at 175 °C
Lemon 200 °C ox	Lemon biomass pre-oxidized at 200 °C

3.2. General Characteristics of Lemon Biomass

Preliminary investigations were conducted to elucidate the thermal characteristics of individual citrus fruit components. From an economic standpoint, practical applications should prioritize the valorization of the entire lemon biomass waste stream, which comprises juice-depleted pulp, albedo, and yellow peel. The biomass waste composition can therefore vary considerably with respect to the relative proportions of individual constituents depending on the source of origin. Heating simulations of samples were performed under inert nitrogen atmosphere (Figure 2) as well as under oxidative conditions (Figure 3).

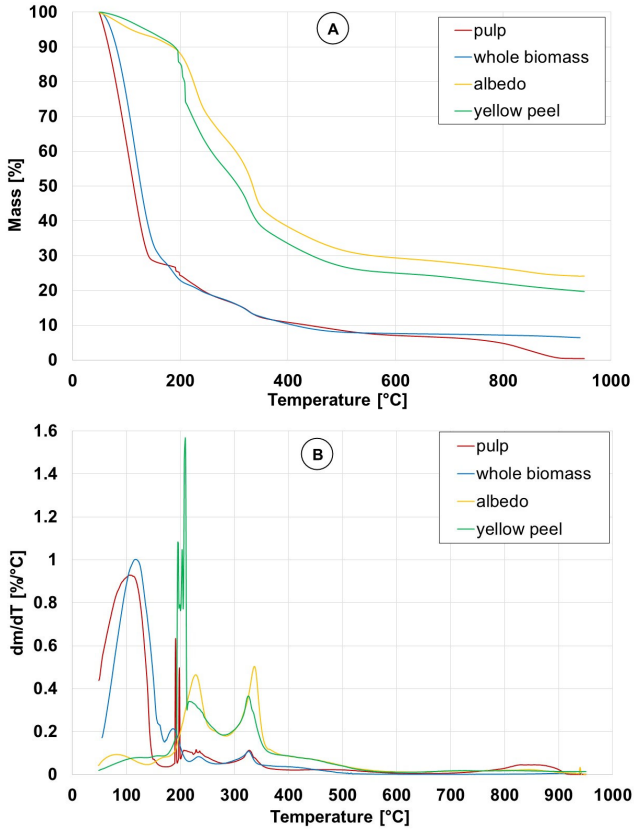


Figure 2. TG (**A**) and DTG (**B**) curves obtained for various components of lemon biomass in a nitrogen atmosphere.

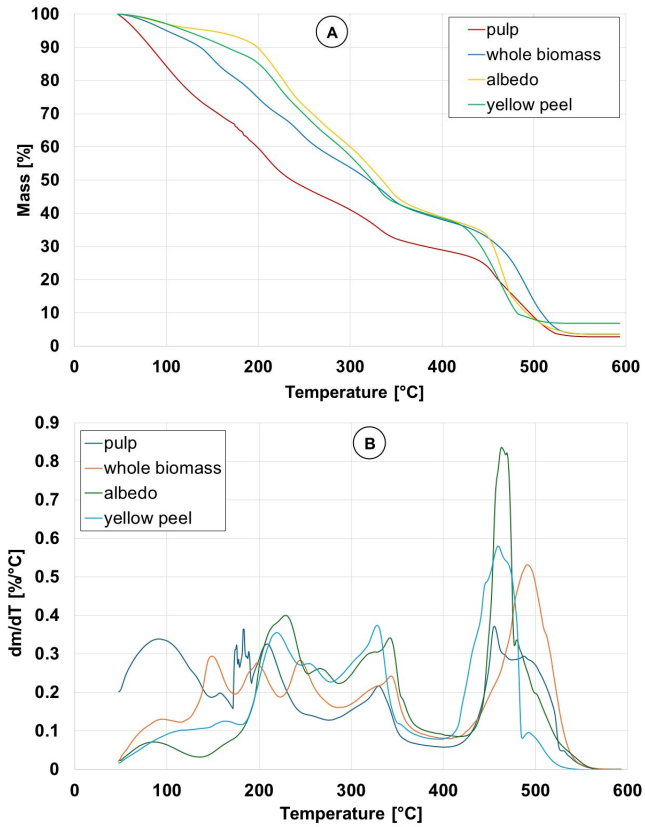


Figure 3. TG (**A**) and DTG (**B**) curves obtained for various components of lemon biomass in an oxidizing atmosphere.

The pulp exhibits the fastest mass loss among all investigated samples in nitrogen atmosphere (Figure 2). The material loses approximately 70% of its mass at a temperature as low as 150 °C. This rapid mass loss indicates a high water content and easily volatilizable organic compounds, such as sugars and organic acids. The characteristic composition of this biomass fraction results in a final residue of merely 0.4% of the initial mass. Yellow peel and albedo degrade at significantly slower rates. The initial mass loss of the peel is comparable to that of pulp; however, the decomposition process proceeds more gradually and extends over a broader temperature range. By 400 °C, approximately 70% of the mass is lost. The yellow peel contains a greater proportion of stable polysaccharidic and lipophilic structures, which are characteristic of the outer portion of the fruit. In contrast, albedo exhibits the slowest degradation and leaves the highest residual mass (24.4%). This indicates a high content of pectin, hemicellulose, and structural carbohydrates, which are more resistant to thermal degradation. Albedo thus possesses the most thermally stable structure among the three main components. The whole biomass demonstrates an intermediate degradation profile between pulp and peel. Although substantial water content is present, the latter portion of the derivative thermogravimetric curve (DTG) is closer to that of the yellow peel, suggesting that the thermal properties of the dried whole biomass will be dominated by the external components of the lemon. In-depth analysis of the DTG curves revealed characteristic decomposition temperatures for the individual structural constituents. The peak observed for pulp at approximately 200 °C corresponds to the degradation of sugars and volatile organic compounds. For the yellow peel, the primary peak occurs in the 200–250 °C range, characteristic of the degradation of lipophilic compounds and waxes typical of this portion of the fruit. For albedo, degradation in this temperature range corresponds to the decomposition of hemicellulose, which contains low-energy bonds. A pronounced thermal decomposition event at approximately 350 °C for both lemon peel and albedo corresponds to the primary decomposition of pectin and cellulose structures. Trace peaks above 600 °C may indicate the final decomposition of aromatic carbon residues. The final stage of thermal decomposition is observed above 800 °C. It is noteworthy that all samples lost their structural integrity after analysis. On the basis of the obtained data, it is concluded that the optimal carbonization temperature should be in the range of 600–800 °C. The range of 600–800 °C is a choice between sufficient carbonization (>600 °C) and preservation of structure (<800 °C). Above this temperature range, undesirable phenomena are observed, including an excessively high ash–carbon ratio, changes in pore structure morphology, loss of valuable oxygen-containing functional groups on the surface, which may be important for adsorption and reactivity, and economic considerations related to the necessity of applying excessive energy for furnace heating [7,30,31].

Thermal stability testing in an oxidizing atmosphere (Figure 3) revealed significant differences compared to tests conducted in nitrogen. The phenomenon of a markedly reduced mass loss of the samples, particularly pronounced at temperatures up to 300 °C, indicates the very significant contribution of oxidation to the concurrently occurring thermal degradation mechanisms. What is more, samples in oxygen atmosphere underwent near-complete combustion by the end of the study leaving only trace amounts of inorganic residue. The pulp contains a high proportion of soluble sugars, pectins, and other hemicelluloses, which decompose in the temperature range of 150–300 °C. These components act as decomposition catalysts, initiating earlier and more intensive mass loss [27–29]. The albedo and yellow represent distinctly more thermally stable components, containing greater proportions of cellulose and lignin structures that require higher temperatures for decomposition. The whole biomass exhibits intermediate thermal characteristics, since it is a mixture of all components. The yellow peel leaves a noticeably larger mass residue (6.8%)

compared to other biomass fractions (approximately 3.6%). This difference is justified by the greater presence of mineral constituents accumulated in the outer layer of the citrus pericarp. More stable fractions delay the overall decomposition process, and the resulting TG/DTG profile reflects the synergistic interaction between components. A critical temperature threshold of approximately 200 °C is observed, above which decomposition of major structural polymers begins. Particularly interesting is the presence of a local maximum on the DTG curve at a temperature of approximately 148 °C, indicating an intense oxidation process. Pre-treatment of biomass below 200 °C is essential for effective carbonization due to selective removal of readily degradable organic components without compromising the lignin and cellulose structures. Importantly, this process can induce the oxidation of functional groups, resulting in the formation of carbonyl, carboxyl, and hydroxyl groups that modify surface properties and material reactivity. Functional groups introduced during oxidative treatment can serve as self-activation agents, creating microporosity even without additional chemical activators [32–34].

3.3. Determination of Water Content

The drying process was carried out until complete water evaporation at 60 °C in an inert atmosphere (Figure 4). Based on the available results, water/moisture content in the tested samples was 3.9% (an additional 1% to reach the set temperature). DSC analysis results (Figure 4) indicate that this constitutes only 17% of the entire phase transition process (water evaporation). Maintaining the temperature at 60 °C does not provide 100% desiccation of the citrus whole biomass.

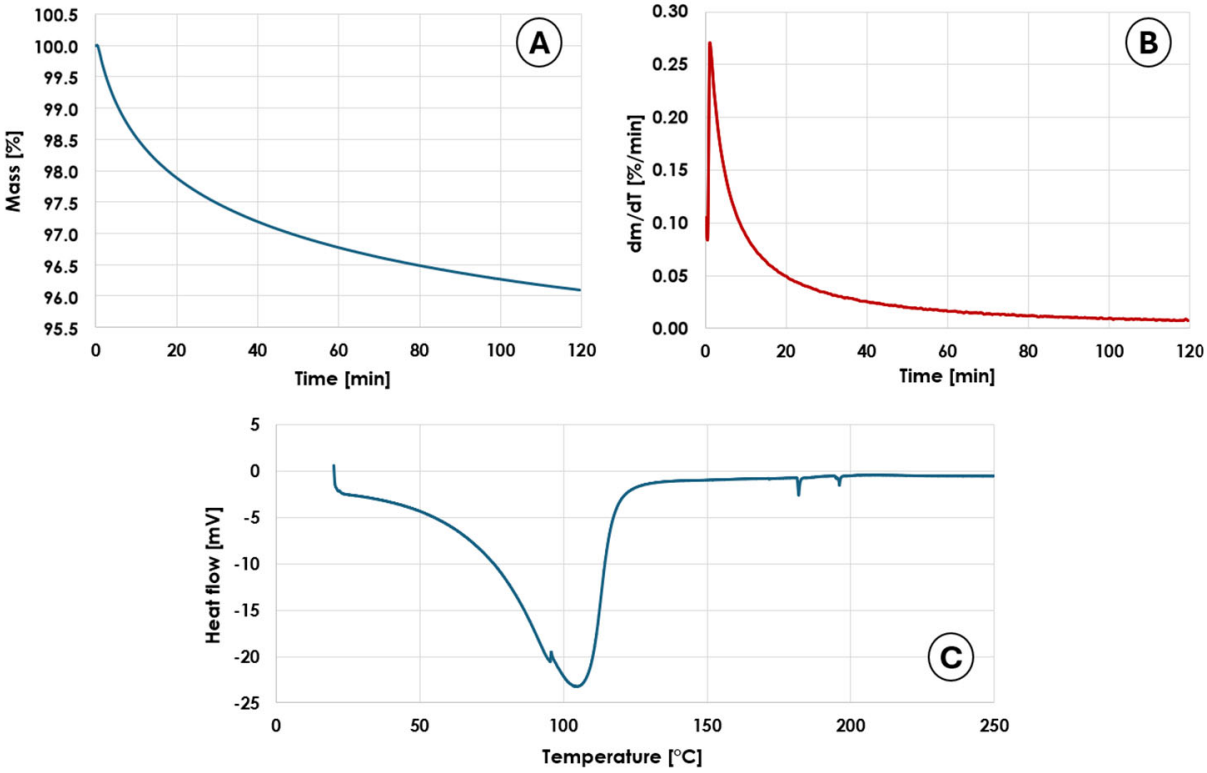


Figure 4. TG and DTG curves (**A**,**B**) obtained for the simulation of the drying process at 60 °C and the DSC curve (**C**) obtained for the lemon biomass sample.

DSC studies of citrus biomass indicate that the evaporation of water begins at the very start of measurement, from 25 °C, and ends at 135 °C. The energy of this transformation is 1250 J/g. Based on literature data (the enthalpy of water evaporation is 2260 J/g), the calculated amount of water evaporated from the citrus precursor up to 135 °C is 57.6%

(Figure 4) (14.75 mg × 0.576 = 8.496 mg of water—which, according to calculations, would require 19.21 J). The total energy recorded for the evaporation process was 18.12 J for 14.5 mg of sample, so calculations indicate that the water content is 8.05 mg, comprising 55% of the total precursor mass. These discrepancies suggest that the first thermal event is primarily due to water evaporation, with only a minor contribution from degradation of the precursor biomass. The results demonstrate that even prolonged drying (2 h for a 15.88 mg sample) of the citrus biomass precursor is insufficient, due to the limited mobility of water within plant cells. Such a drying process would require higher energy input to achieve complete removal of water from the precursor. The aim of this study is to reflect the processing conditions of biomass for potential applications, and hence the use of a conventional air-drying oven was selected. However, previous TG studies indicated that increasing the drying temperature is associated with the risk of initiating oxidation processes. Therefore, for subsequent experiments, a drying temperature of 60 °C and a duration of 2 h were selected for the citrus biomass.

3.4. Preliminary Oxidation Process

3.4.1. Selection of Oxidation Time and Thermal Characteristics of the Oxidation Process

Preliminary research has demonstrated that the oxidation temperature of citrus biomass should not exceed 200 °C due to the onset of thermal decomposition of the main constituents. Since water loss in the sample was predominantly observed up to 100–120 °C, it was decided to investigate the temperature range around the first subsequent distinct thermal decomposition event occurring at approximately 150 °C. To determine the time required for the pre-oxidation process, thermogravimetric (TG) and derivative thermogravimetric (DTG) curves (Figure 5) simulating a 30-min process were subjected to detailed analysis.

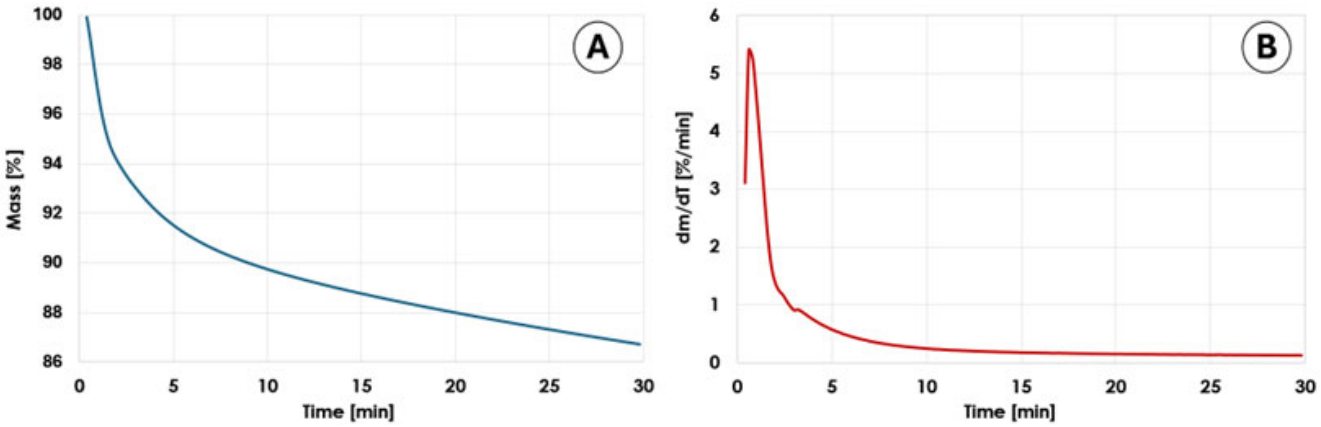


Figure 5. TG and DTG curves (**A**,**B**) obtained for the isothermal simulation of the preliminary oxidation process of lemon biomass at 150 °C.

The study demonstrated that the oxidation process rate is the highest in the first 5 min, and next the rate gradually decreases. Simulation indicated that 3 min could be optimal for small samples oxidized under standard conditions. Excessive dwell time may lead to a series of undesirable phenomena, such as the onset of degradation of the main polymer matrix, which would not be able to create during the subsequent carbonization in an oxygen-free environment a dense carbon structure with a favorable pore distribution. The next part aimed to verify the oxidation rate of the sample at different temperatures. Standard oxidation was performed at temperatures of 120, 140, 150, 160, 175, and 200 °C, as shown in the TG and DTG curves (Figure 6). A tendency was observed where increasing the temperature increased the intensity of mass loss of the sample and accelerated its onset.

The maximum process intensity was observed in the first minute. The curves obtained for samples oxidized at 140, 150, and 160 °C showed similar behavior and were characterized by mass loss of approximately 8% relative to the initial sample mass. The smallest mass loss was observed for the sample oxidized at 120 °C, amounting to approximately 6%, while the largest was for the sample oxidized at 200 °C, amounting to 13.6%.

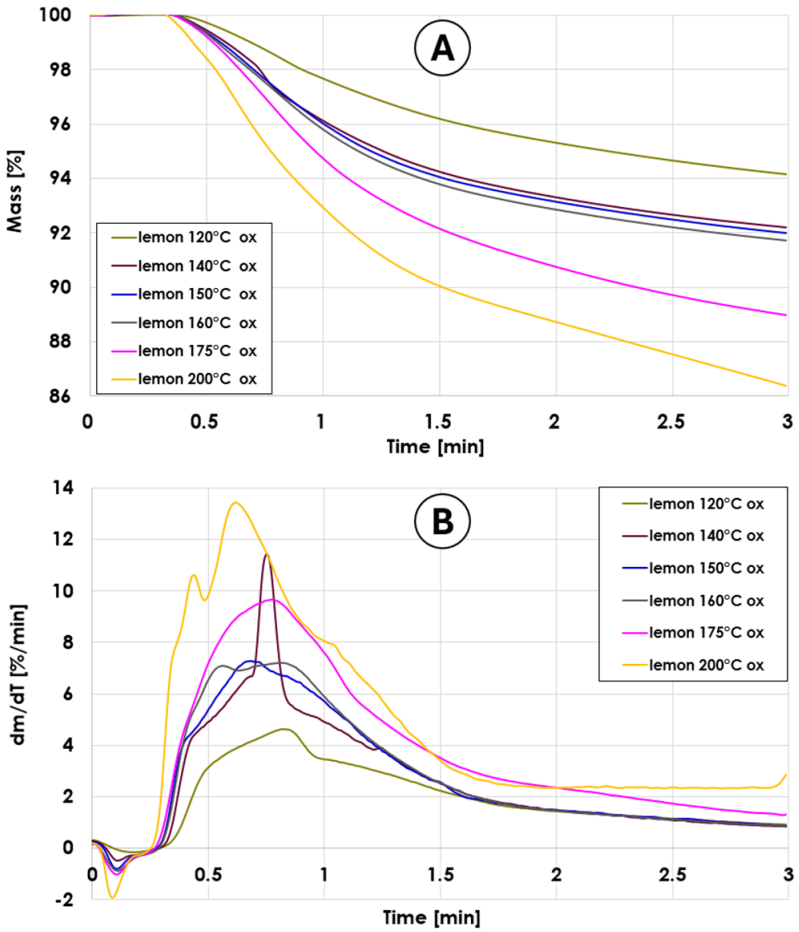


Figure 6. TG (**A**) and DTG (**B**) curves obtained for lemon biomass samples oxidized at temperatures ranging from 120 to 200 °C for 3 min.

3.4.2. The Effect of Pre-Oxidation on Structural Changes (FTIR)

FTIR analysis (Figure 7) demonstrates that the oxidation treatment process exerts a direct influence on the structural changes of the material relative to the reference sample, which was the untreated citrus biomass. The most visible structural changes are observed in the oxidation temperature samples at 140 °C and 150 °C. A distinctive absorption bands appear at approximately 3100 cm^{-1}, corresponding to aromatic C–H stretching vibrations. In the 1600–1700 cm^{-1} region, characteristic aromatic C=C stretching vibrations are evident, with particular significance attributed to the peak at 1664 cm^{-1}, which exhibits a pronounced decrease in intensity for samples oxidized above 160 °C. Additionally, a prominent absorption band at 891 cm^{-1} is observed, assigned to aromatic C–H bending vibrations within aromatic ring structures. The appearance of a distinct bonds at approximately 1731 cm^{-1} indicates the presence of C=O bonds characteristic of carbonyl groups, while bands in the 1100–1200 cm^{-1} region confirm C–O bonds typical of ether and hydroxyl functional groups. Spectra in the 400–640 cm^{-1} region further support the presence of aromatic structural components. A notable decrease in peak intensities within the 2800–3000 cm^{-1} region (aliphatic C–H stretching vibrations) is observed for samples oxidized at 160 °C, 175 °C, and 200 °C. This attenuation is consistent with progressive

carbonization-related degradation processes. The observed spectroscopic changes reveal a direct correlation between the temperature of oxidation and the chemical structure of the samples, indicating distinct stages of thermal degradation: initial stage (120 °C)—elimination of residual moisture and initial decomposition of sugars and cellulose occur (which is correlated with TG results); intermediate stage (140–150 °C)—condensation and aromatization of organic compounds take place (these samples represent the optimal conditions for subsequent investigations, as they exhibit enhanced aromatic character while maintaining structural integrity); transition stage (160 °C and above)—progressive decrease in functional group content of oxygen- and hydrogen-rich; advanced stage (200 °C)—the spectroscopic data indicate the onset of advanced carbonization, associated with degradation of the polymeric macromolecular structure comprising the biomass. Based on the foregoing analysis, an oxidation temperature of 140 °C was selected for subsequent experimental work. The IR spectrum of this sample exhibits characteristics very similar to those of the 150 °C sample, while simultaneously providing a safer operational margin for minor temperature fluctuations associated with thermal equipment inertia, heating stability, and instrumentation variability. This selection strategy also requires a lower input of thermal energy, which directly translates to potential cost savings in practical applications.

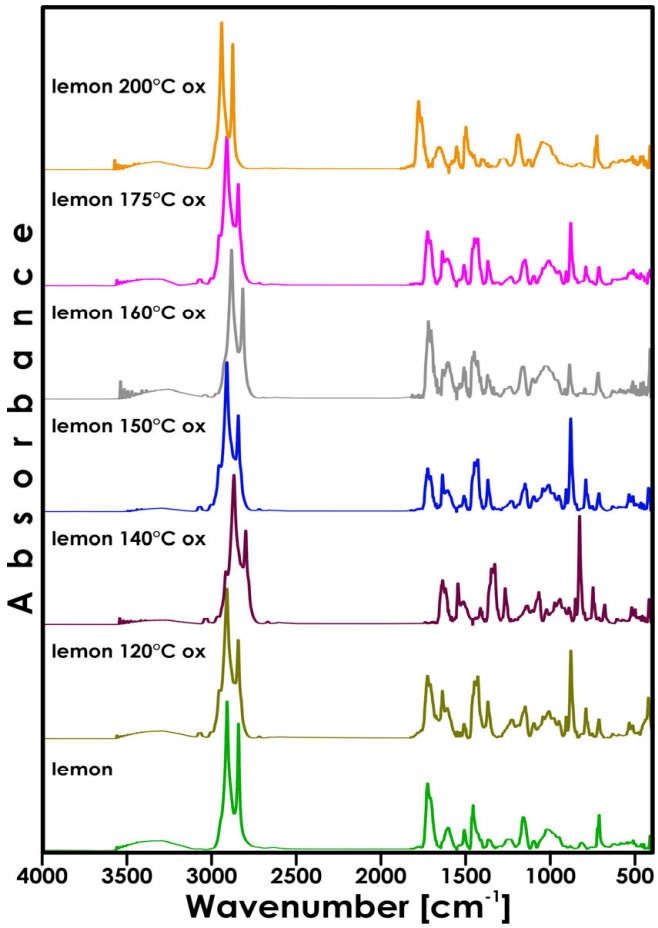


Figure 7. FTIR spectra obtained for samples oxidized in the range of 120–200 °C and an unoxidized reference sample of lemon biomass.

3.5. Carbonization

The results of thermal characteristics measurements conducted under non-oxidant conditions for lemon biomass samples demonstrated that the optimal carbonization temperature is approximately 700 °C. To optimize the process, samples pre-oxidized at 140 °C were heated to the temperatures from the range of 600, 650, 700, 750 and 800 °C. The samples

were heated in a TGA furnace at a heating rate of 10 K/min until the target temperature. Attention was paid to the mass residue, the values of which are summarized in Table 2, while the thermogravimetric curves are presented in Figure 8. Subsequently, to verify the effect of pyrolysis temperature on physicochemical properties, the electrical conductivity of the resulting carbonized materials was measured, and the results are presented in Table 2.

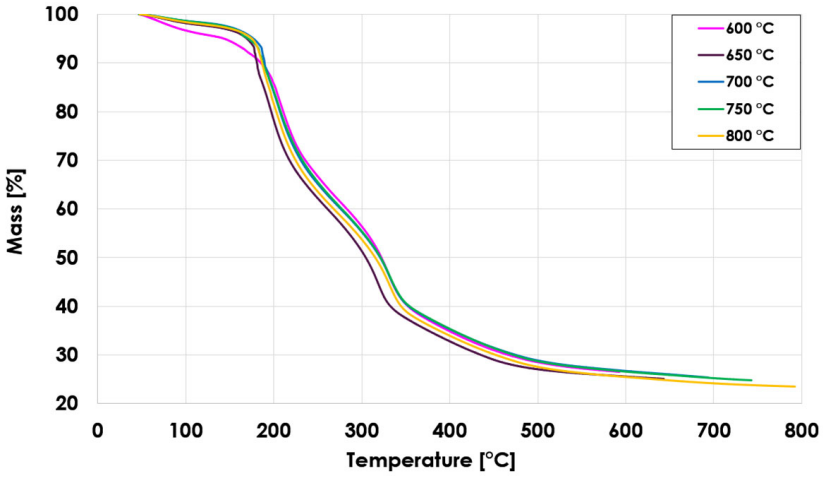


Figure 8. TG curves obtained for carbonization process to the range of 600–800 °C of pre-oxidized biomass samples at a temperature of 140 °C.

Table 2. Mass residue of samples after TG simulations and surface resistance.

Upper Temperature Limit of Carbonization Process [°C]	Residual Mass [%]	Sheet Resistance [Ω/sq]
600	26.50	2375.80 ± 261.39
650	25.12	153.00 ± 19.85
700	25.39	30.85 ± 3.76
750	24.85	127.37 ± 16.51
800	23.50	5397.00 ± 493.67

As hypothesized, higher target temperatures generally resulted in decreased residual mass of the samples. An exception to this trend was observed for the sample carbonized to 650 °C, whose main thermal decomposition stage commenced approximately 10–15 °C earlier compared to the other materials. Furthermore, the thermal decomposition profile of the sample carbonized at 600 °C showed a notable deviation from the other samples in the initial temperature range up to 200 °C. These findings indicate that biomass derived from even the same batch of citrus fruits exhibits certain variations in physicochemical structure. A well-designed process for the preparation of carbon materials, particularly for practical applications, should account for this phenomenon by averaging results and allowing for the selection of optimal processing conditions that are universal for biomass sources, which may prove to be more or less heterogeneous. The difference between the highest residual mass obtained for the sample carbonized to 800 °C and the lowest obtained to 600 °C was 3%. In particular, all carbonized biochars retained their intact structure. The lowest resistance was achieved for the material carbonized to 700 °C. The observed trend is consistent with literature data describing the application of biomass for the preparation of carbon materials used, among other applications, in the synthesis of supercapacitors [35–38]. The electrical conductivity of carbon biochars derived from citrus biomass increases by several orders of magnitude in the temperature range of 600 to 800 °C, mainly due to the achievement of the percolation threshold (~600 °C), through which a three-dimensional network of interconnected conductive carbon pathways is formed,

and the reduction in the band gap energy, which facilitates electron transport through electron jumping and tunneling mechanisms. This process is promoted by intensive graphitization of the material—characterized by an improvement in the ordering of the crystalline structure, reduction in structural defects, and elimination of oxygen-containing functional groups, which occur intensively between 650 and 750 °C. For samples carbonized to 700 °C, an optimal balance is achieved between high electrical conductivity and the preserved porosity of the material, which explains the decrease in electrical conductivity at higher temperatures.

3.6. The Influence of Oxidation Conditions on the Final Structure of Carbonized Material

3.6.1. Thermal Stability

Samples pre-oxidized in the temperature range of 120 °C to 200 °C were subjected to non-oxidant carbonization to 700 °C. The reference sample consisted of pre-dried citrus biomass (60 °C, 2 h). The results were presented in Figure 9 and Table 3. Initially, mass loss associated with residual water was observed, particularly pronounced for lemon and lemon 120 °C ox samples. A correlation was found between increased thermal stability of the samples and the pre-oxidation temperature. The reference sample exhibited a final residue of 17.66% of the initial mass and was the only sample that did not retain a coherent structure. For the lemon 120 °C ox, lemon 140 °C ox, and lemon 150 °C ox samples, an increase in residual mass of approximately 50% relative to the reference was observed. Above a pre-oxidation temperature of 150 °C, a decrease in the residue content was observed after carbonization. This observation indicates that excessive oxygen was supplied to the sample, leading to premature thermal decomposition already during the pre-oxidation process.

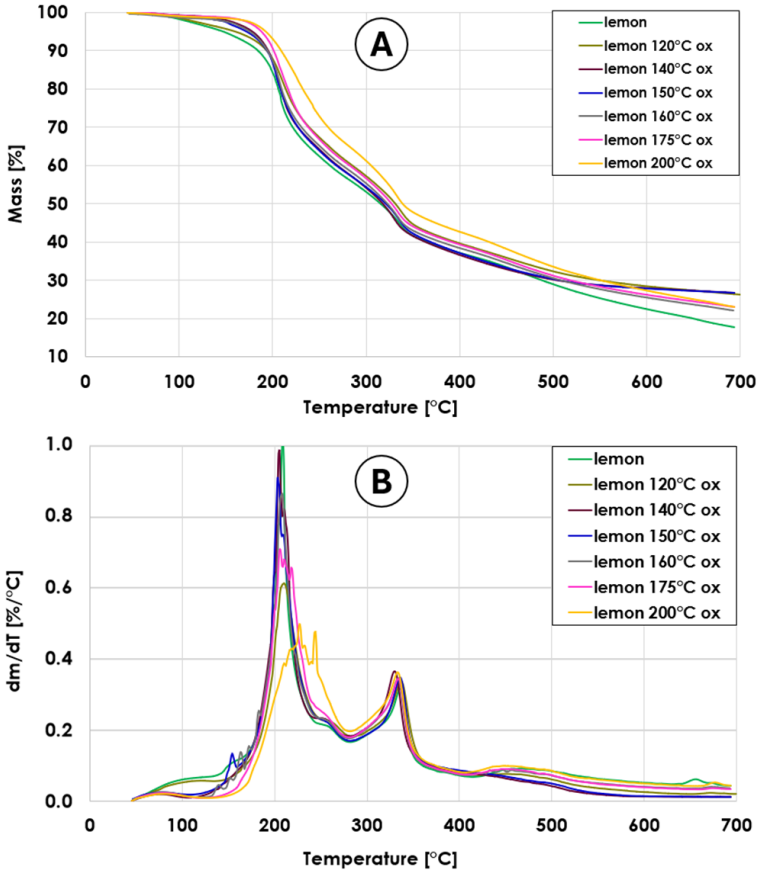


Figure 9. TG (**A**) and DTG (**B**) curves obtained for the simulation of the carbonization process of samples previously oxidized at 120–200 °C and for the reference sample of lemon biomass.

Table 3. Summary of thermal degradation data from TG analysis.

Sample	Residual Mass [%]	T_{onset} of Mass Loss [°C]	T_{DTGmax} 1 [°C]	T_{DTGmax} 2 [°C]
Lemon	17.66	138	209	336
Lemon 120 °C ox	26.31	146	209	337
Lemon 140 °C ox	26.58	149	204	330
Lemon 150 °C ox	26.64	151	203	336
Lemon 160 °C ox	22.18	153	207	333
Lemon 175 °C ox	23.02	162	212	334
Lemon 200 °C ox	22.96	167	227	333

3.6.2. Thermal Properties Analysis of Carbonizates

DSC studies of carbonizates (Figure 10) reveal that they readily adsorb water, with a distinct endothermic peak corresponding to water evaporation evident in the first DSC scan. A notable observation emerges in the second scan, where pronounced melting peaks are observed from phases originating from compounds such as sugars, pectins, and their derivatives. During biomass carbonization under controlled/moderate-temperature carbonization conditions, simple sugars (glucose, fructose) can undergo caramelization and polymerization, forming carbohydrate polymers. These sugar-derived carbons exhibit phase transitions and structural rearrangements in the temperature range of 200–300 °C [39]. Particularly in lemon carbonizates, which are rich in natural sugars, partially caramelized products may be present, exhibiting endothermic transitions at approximately 200–250 °C associated with the decomposition of amorphous structures. Lemon biomass contains natural polysaccharides (pectins, arabinogalactans) that may not be completely degraded during the carbonization process. The thermal transitions of starch and polysaccharide derivatives occur in the range of 60–160 °C for gelatinization; however, retrogradation and structural transitions can also take place at temperatures up to 300 °C. In biochar, these residual components can exhibit crystallization transitions and structural reorganizations in the temperature range of 200–300 °C [40].

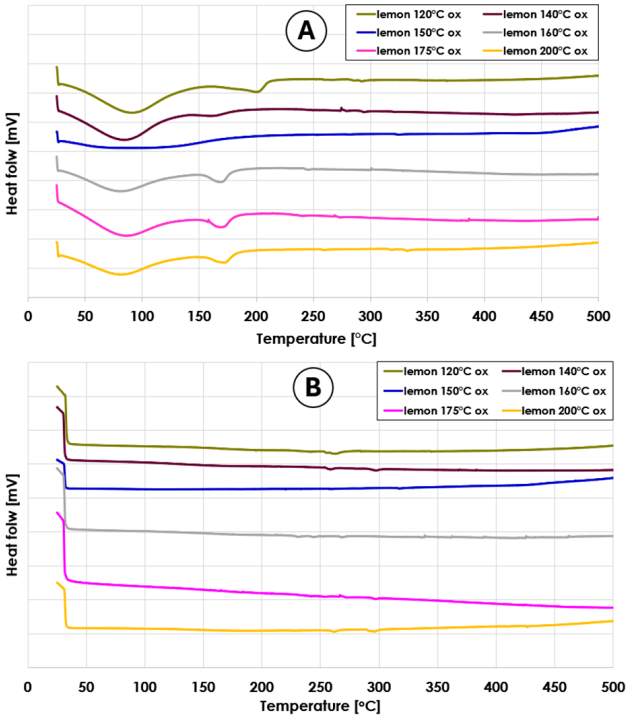


Figure 10. Differential scanning calorimetry analysis: first (**A**) and second (**B**) heating scans of oxidatively pre-treated lemon biomass.

3.6.3. Morphological and Elemental Characterization of Carbon Carbonizates (SEM and EDS)

The presented SEM images (Figure 11) reveal significant differences in morphology and porous structure of carbon materials as a function of pre-oxidation temperature. Microstructural analysis indicates substantial changes in the pore architecture, wall thickness, and overall structural quality of the carbon. Carbonizates pre-oxidized at 120 °C exhibit a compact and dense structure. For samples oxidized at 140 °C and 150 °C, a highly porous, three-dimensional structure resembling porous biochar or aerogel is evident, featuring numerous macropores (10–100 μm) and mesopores. The wall surface displays additional microporosity, thereby increasing the total specific surface area of the material. As evidenced by previous studies, mild pre-oxidation introduces oxygen-containing functional groups (hydroxyl, carboxyl, and carbonyl) onto the precursor surface without excessive structural damage. During subsequent carbonization, these groups undergo decomposition, releasing volatile products (H_2O, CO, CO_2), which create and stabilize the porous structure. This process prevents excessive densification of the material during carbonization, yielding a favorable structure for further applications. At higher pre-oxidation temperatures, we observe an increase in structural densification accompanied by marked morphological changes. The pores become noticeably less regular. The material oxidized at the highest temperature demonstrates the most densified and compact structure, exhibiting significant densification with sparse and small pores. This trend reversal can be explained by the fact that high-temperature oxidation leads to intensive removal of aliphatic structures and oxygen-containing functional groups, causing premature carbonization and structural reorganization. During proper carbonization, the material is already sufficiently ordered that pore expansion does not occur—rather, further densification is observed. Such material is clearly unsuitable for applications requiring high specific surface area. EDS analysis revealed a dependence of decreasing carbon content on the surface with increasing pre-oxidation temperature at the expense of other elements (Table 4). A threefold increase in oxygen is observed for the sample oxidized at 200 °C relative to the optimal sample at 140 °C. Simultaneously, a significant increase in potassium is observed. These facts indicate the presence of inorganic compounds in the samples. Based on available literature analysis, it is concluded that the dominant compounds forming the mineral phase corresponding to carbonization at 700 °C are K_2CO_3, $CaCO_3$, $K_2Ca(CO_3)_2$, and CaO [41–43].

Table 4. Energy Dispersive Spectroscopy Analysis: Elemental composition of carbon carbonizate samples.

Sample Name	Parameter [%]	Elements									
		C	**O**	**Na**	**Mg**	**Si**	**P**	**S**	**K**	**Ca**	**Al**
Lemon 120 °C ox	Weight	65.62	15.76	0.73	0.92	1.89	1.04	0.91	8.08	5.03	-
	Uncertainty	5.88	8.93	12.92	11.66	9.62	19.92	18.54	7.42	10.47	-
Lemon 140 °C ox	Weight	56.15	11.93	1.06	1.23	-	2.81	2.84	15.04	8.94	-
	Uncertainty	6.84	10.12	12.07	11.36	-	7.43	6.93	6.01	8.65	-
Lemon 150 °C ox	Weight	54.93	11.81	-	1.81	-	2.25	6.49	16.82	6.53	-
	Uncertainty	7.28	9.97	-	10.21	-	8.56	5.53	5.45	9.98	-
Lemon 160 °C ox	Weight	46.33	7.96	-	1.51	2.15	3.30	-	27.89	10.86	-
	Uncertainty	6.97	12.40	-	9.79	8.80	6.60	-	5.17	8.62	-
Lemon 175 °C ox	Weight	47.55	20.63	0.28	1.00	-	1.52	0.94	20.16	7.92	-
	Uncertainty	6.09	8.96	34.97	12.12	-	14.80	23.06	5.18	9.90	-
Lemon 200 °C ox	Weight	24.42	32.62	0.62	0.48	2.39	-	-	36.08	2.12	1.28
	Uncertainty	6.67	8.07	13.56	17.35	8.75	-	-	4.26	19.83	10.90

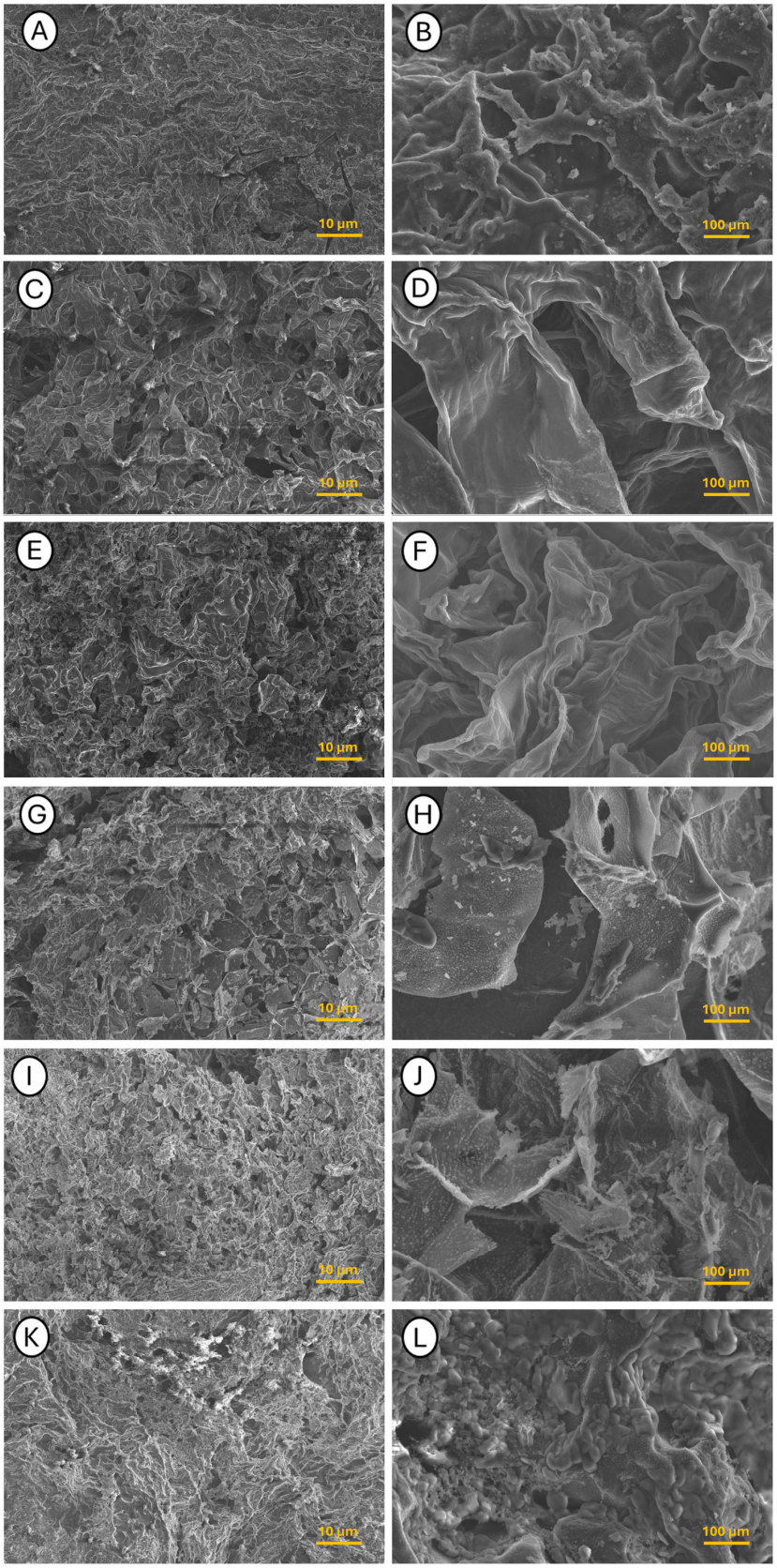


Figure 11. Pictures of samples: lemon 120 °C ox taken at a blow-up of 500× (**A**) and 5000× (**B**); lemon 140 °C ox taken at a blow-up of 500× (**C**) and 5000× (**D**); lemon 150 °C ox taken at a blow-up of 500× (**E**) and 5000× (**F**); lemon 160 °C ox taken at a blow-up of 500× (**G**) and 5000× (**H**); lemon 175 °C ox taken at a blow-up of 500× (**I**) and 5000× (**J**); lemon 200 °C ox taken at a blow-up of 500× (**K**) and 5000× (**L**).

3.6.4. Surface Resistivity of Carbon Materials

Carbon materials obtained through lemon biomass carbonization exhibited a distinctly nonlinear dependence of sheet resistance on oxidative pre-heating temperature (Table 5), characterized by a drastic anomaly at 160 °C (4503 Ω/sq), where the sheet resistance increased 145-fold relative to the optimally oxidized sample treated at 140 °C (30.849 Ω/sq). The sample subjected to treatment at 140 °C exhibited the lowest sheet resistance, indicating an equilibrium point between selective graphitization of the material structure and controlled introduction of oxygen-containing functional groups. The anomaly at 160 °C may result from disruption of the percolation network—this temperature represents a bifurcation point at which accumulation of structural defects and the presence of mineral substances leads to fragmentation of coherent conductive pathways. This phenomenon is consistent with SEM observations, where the material structure is markedly degraded compared to samples oxidized at lower temperatures. Higher temperatures (175–200 °C) enable decomposition of unstable oxygen-containing groups and regeneration of graphitization; however, due to structural hysteresis, these samples do not recover the optimal sheet resistance achieved at 140 °C. Additionally, they are characterized by high mineral substance content, which disrupts the conduction process. Conductivity increases by several orders of magnitude between 600 and 800 °C, mainly due to the increased proportion of the carbon phase and the reduction in interparticle resistance [44–47].

Table 5. Sheet resistance values for carbon carbonizates.

Sample	Sheet Resistance [Ω/sq]
Lemon 120 °C ox	1271.70 ± 165.32
Lemon 140 °C ox	30.85 ± 3.76
Lemon 150 °C ox	205.31 ± 21.59
Lemon 160 °C ox	4503.00 ± 395.30
Lemon 175 °C ox	3362.20 ± 372.84
Lemon 200 °C ox	3414.70 ± 427.06

4. Conclusions

This study investigated the optimization potential of porous carbon material formation through incorporation of a pre-oxidation step to obtain functional and dense structures. The physicochemical and surface properties of the obtained materials were characterized. Pre-oxidation of the biomass matrix below 200 °C constitutes a critical thermal-oxidative pretreatment in the process of obtaining porous carbon materials, with the primary objective of optimizing material structure prior to main carbonization. This step selectively removes readily decomposable fractions without damaging the carbon skeleton, while simultaneously modifying the structure of cellulose and lignin, rendering them more reactive. Consequently, significant benefits are achieved: improved structural retention during drying due to removal of soluble fractions, more homogeneous and regular porosity in place of large structural defects, enhanced mechanical properties enabling better retention of characteristics up to carbonization temperatures, and increased specific surface area of the final samples after carbonization. Precise control of the pretreatment temperature enables gradual and controlled matrix decomposition rather than abrupt thermal transitions, ultimately yielding high-quality carbon materials with superior performance properties. Moreover, the pre-oxidation temperature of the biomass directly controls the morphology and pore size distribution in the final carbon material. At temperatures below 150 °C, oxidation proceeds primarily at the surface, leading to uniform development of micro- and mesopores. This structure promotes high conductivity through the maintenance of coherent conductive pathways. The sample pre-oxidized at 140 °C presented in this study exhibits

a sheet resistance of 30 Ω/sq, which represents a favorable value for carbonized carbon materials. Compared to conventional carbon materials, the measured sheet resistance falls within a range slightly higher than conventional graphitized materials (0.05–20 Ω/sq), while being lower than unactivated carbon aerogels based on precursors of resorcinol-formaldehyde (RF) precursors (100–250 Ω/sq) [48,49]. The electrical conductivity value obtained for the material suggests effective carbonization and good electrical connectivity within the material structure, rendering it potentially suitable for electrochemical applications, such as porous supercapacitor electrodes or thermal energy storage systems capable of, among other functionalities, electrothermal conversion.

Author Contributions: Conceptualization, R.T. and K.P.; methodology, R.T. and K.P.; software, R.T.; validation, R.T. and K.P.; formal analysis, R.T.; investigation, R.T.; resources, K.P.; data curation, R.T.; writing—original draft preparation, R.T.; writing—review and editing, K.P.; visualization, R.T.; supervision, K.P.; project administration, K.P.; funding acquisition, K.P. All authors have read and agreed to the published version of the manuscript.

Funding: The authors are grateful to the Polish National Science Centre for financial support under Contract No. 2023/51/B/ST8/02745. This work was supported by a subsidy from the Ministry of Education and Science for the AGH University of Science and Technology in Kraków (Project No. 16.16.160.557).

Data Availability Statement: The original data presented in the study will be openly available in AGH Repository.

Acknowledgments: During the preparation of this manuscript/study, the authors used Perplexity AI (Perplexity AI, Inc., San Francisco, CA, USA) for the purposes of creating images for the research work diagram (Figure 1). The authors have reviewed and edited the output and take full responsibility for the content of this publication.

Conflicts of Interest: The authors declare no conflicts of interest.

References

1. Shen, Y.; Yang, J. Progress in the Synthesis of Carbon Aerogels for Advanced Energy Storage Applications. *Green Chem.* **2024**, *26*, 8969–9004. [CrossRef]
2. Imran, M.; Chew, J.W. Upcycling Citrus Waste into Porous Carbon and Aerogel Materials: State-of-the-Art and Prospects. *Carbon. Capture Sci. Technol.* **2025**, *16*, 100462. [CrossRef]
3. Bari, G.A.K.M.R.; Jeong, J.-H. Potential of Carbon Aerogels in Energy: Design, Characteristics, and Applications. *Gels* **2024**, *10*, 389. [CrossRef]
4. Xi, W.; Lu, J.; Qun, J.; Jiao, B. Characterization of Phenolic Profile and Antioxidant Capacity of Different Fruit Part from Lemon (*Citrus limon* Burm.) Cultivars. *J. Food Sci. Technol.* **2017**, *54*, 1108–1118. [CrossRef]
5. Tinh, N.T.T.; Sitolo, G.C.; Yamamoto, Y.; Suzuki, T. *Citrus limon* Peel Powder Reduces Intestinal Barrier Defects and Inflammation in a Colitic Murine Experimental Model. *Foods* **2021**, *10*, 240. [CrossRef]
6. Klimek-Szczykutowicz, M.; Szopa, A.; Ekiert, H. *Citrus limon* (Lemon) Phenomenon—A Review of the Chemistry, Pharmacological Properties, Applications in the Modern Pharmaceutical, Food, and Cosmetics Industries, and Biotechnological Studies. *Plants* **2020**, *9*, 119. [CrossRef]
7. Nieto, G.; Fernández-López, J.; Pérez-Álvarez, J.A.; Peñalver, R.; Ros-Berruezo, G.; Viuda-Martos, M. Valorization of Citrus Co-Products: Recovery of Bioactive Compounds and Application in Meat and Meat Products. *Plants* **2021**, *10*, 1069. [CrossRef] [PubMed]
8. Kim, S.Y. Chemical Composition and Antioxidant Activity of Crude Polysaccharide from Citron (*Citrus junos* Sieb. Ex TANAKA) Seed. *Prev. Nutr. Food Sci.* **2018**, *23*, 335–340. [CrossRef]
9. Kumar, A.; Kumari, L.; Laghari, A.A.; Rong, H.; Jamro, I.A.; Sajnani, S.; Aborisade, M.A.; Rajput, G.; Oba, B.T.; Nkinahamira, F.; et al. Exploring the Integrated Potential of Pyrolysis and Low-Temperature Wet Torrefaction for Typical Medical Waste Valorization: A Multifaceted Approach Leveraging Online TG-FTIR-MS, 2D-COS, Iso-Conversional Kinetics, and Reaction Mechanisms. *Chem. Eng. J.* **2024**, *499*, 156464. [CrossRef]
10. Kozyatnyk, I.; Benavente, V.; Weidemann, E.; Gentili, F.G.; Jansson, S. Influence of Hydrothermal Carbonization Conditions on the Porosity, Functionality, and Sorption Properties of Microalgae Hydrochars. *Sci. Rep.* **2023**, *13*, 8562. [CrossRef]

11. Magalhães, D.; Vilas-Boas, A.A.; Teixeira, P.; Pintado, M. Functional Ingredients and Additives from Lemon By-Products and Their Applications in Food Preservation: A Review. *Foods* **2023**, *12*, 1095. [CrossRef]
12. Xu, Q.; Guan, B.; Guo, W.; Liu, X. Effect of Antioxidants on Thermo-Oxidative Stability and Aging of Bio-Based PA56T and Fast Characterization of Anti-Oxidation Performance. *Polymers* **2022**, *14*, 1280. [CrossRef]
13. Kundu, A.; Basu, S.; Maity, B. Upcycling Waste: *Citrus limon* Peel-Derived Carbon Quantum Dots for Sensitive Detection of Tetracycline in the Nanomolar Range. *ACS Omega* **2023**, *8*, 36449–36459. [CrossRef] [PubMed]
14. Liu, H.; Feng, H.; Chu, P.; Xie, W.; Wang, X.; Zhang, Z.; Wang, S. A Coral-like Skeleton Carbon Aerogel Achieves Good Mechanical and Thermal Insulation Properties. *Ceram. Int.* **2024**, *50*, 42119–42126. [CrossRef]
15. Liu, X.; Lin, J.; Zhao, Z.; Min, Y.; Song, J.; Li, B.; Huang, J. Advances in Functional Applications of Biomass-Derived Carbon Composites for Phase Change Materials. *Microstructures* **2025**, *5*, 2025039. [CrossRef]
16. Ahmad, A.; Navarro, H.; Ghosh, S.; Ding, Y.; Roy, J.N. Evaluation of New PCM/PV Configurations for Electrical Energy Efficiency Improvement through Thermal Management of PV Systems. *Energies* **2021**, *14*, 4130. [CrossRef]
17. Zhao, Z.; Feng, D.; Zhang, X.; Feng, Y. Ultra-Compact Cellular Structured Bio-Carbon Aerogels Supported PCM for Exceptional Thermal Insulation and Radiation Shielding for Space Applications. *Energy Environ. Mater.* **2025**, *8*, e70042. [CrossRef]
18. Nie, J.; Feng, D.; Shang, J.; Nasen, B.; Jiang, T.; Liu, Y.; Hou, S. Green Composite Aerogel Based on Citrus Peel/Chitosan/Bentonite for Sustainable Removal Cu(II) from Water Matrices. *Sci. Rep.* **2023**, *13*, 15443. [CrossRef]
19. Ma, H.; Zhang, Y.; Qiu, L.; Li, W.; Sun, R.; Zhu, M.; Yang, X. Effect of Reaction Conditions on Energy Yield of Pyrolysis Gas from Apple Tree Branches. *ACS Omega* **2024**, *9*, 28028–28036. [CrossRef]
20. Igliński, B.; Kujawski, W.; Kiełkowska, U. Pyrolysis of Waste Biomass: Technical and Process Achievements, and Future Development—A Review. *Energies* **2023**, *16*, 1829. [CrossRef]
21. Mishra, R.K.; Misra, M.; Mohanty, A.K. Value-Added Bio-Carbon Production through the Slow Pyrolysis of Waste Bio-Oil: Fundamental Studies on Their Structure–Property–Processing Co-Relation. *ACS Omega* **2022**, *7*, 1612–1627. [CrossRef] [PubMed]
22. Chakraborty, S.; Aktay, N.; Alptekin, F.M.; Celiktas, M.S.; Dunford, N.T. Effect of Process Parameters and Biomass Type on Properties of Carbon Produced by Pyrolysis. *Biomass* **2025**, *5*, 52. [CrossRef]
23. Kiełbasa, K.; Siemak, J.; Sreńscek-Nazzal, J.; Benaouda, B.; Roy, B.; Michalkiewicz, B. Carbon Dioxide Adsorption over Activated Biocarbons Derived from Lemon Peel. *Molecules* **2024**, *29*, 4183. [CrossRef]
24. Emrooz, H.B.M.; Hosseini Naghavi, M.S.; Mohammadi, S.; Mousavi-Khoshdel, S.M. One-Step Green Synthesis of Meso-Microporous Carbons by Self-Activation of Lemon Wastes for High-Performance Supercapacitors. *J. Energy Storage* **2022**, *56*, 105989. [CrossRef]
25. Twaróg, R.; Szatkowski, P.; Pielichowska, K. Phase Change Materials in Electrothermal Conversion Systems: A Review. *Energies* **2025**, *18*, 569. [CrossRef]
26. Vilén, A.; Laurell, P.; Vahala, R. Comparative Life Cycle Assessment of Activated Carbon Production from Various Raw Materials. *J. Environ. Manag.* **2022**, *324*, 116356. [CrossRef]
27. Zhao, L.; Cao, X.; Zheng, W.; Kan, Y. Phosphorus-Assisted Biomass Thermal Conversion: Reducing Carbon Loss and Improving Biochar Stability. *PLoS ONE* **2014**, *9*, e115373. [CrossRef] [PubMed]
28. Cho, M.; Ko, F.K.; Renneckar, S. Impact of Thermal Oxidative Stabilization on the Performance of Lignin-Based Carbon Nanofiber Mats. *ACS Omega* **2019**, *4*, 5345–5355. [CrossRef] [PubMed]
29. Chen, Y.; Sun, H.; He, X.; Chen, Q.; Zhao, J.; Wei, Y.; Wu, X.; Zhang, Z.; Jiang, Y.; Chou, S. Pre-Oxidation Strategy Transforming Waste Foam to Hard Carbon Anodes for Boosting Sodium Storage Performance. *Small* **2024**, *20*, 2307132. [CrossRef]
30. Escobedo-Avellaneda, Z.; Gutiérrez-Uribe, J.; Valdez-Fragoso, A.; Torres, J.A.; Welti-Chanes, J. Phytochemicals and Antioxidant Activity of Juice, Flavedo, Albedo and Comminuted Orange. *J. Funct. Foods* **2014**, *6*, 470–481. [CrossRef]
31. Munir, H.; Yaqoob, S.; Awan, K.A.; Imtiaz, A.; Naveed, H.; Ahmad, N.; Naeem, M.; Sultan, W.; Ma, Y. Unveiling the Chemistry of Citrus Peel: Insights into Nutraceutical Potential and Therapeutic Applications. *Foods* **2024**, *13*, 1681. [CrossRef]
32. Lee, S.M.; Lee, S.H.; Jung, D.-H. Surface Oxidation of Petroleum Pitch to Improve Mesopore Ratio and Specific Surface Area of Activated Carbon. *Sci. Rep.* **2021**, *11*, 1460. [CrossRef] [PubMed]
33. Zhou, J.; Yang, P.; Kots, P.A.; Cohen, M.; Chen, Y.; Quinn, C.M.; de Mello, M.D.; Anibal Boscoboinik, J.; Shaw, W.J.; Caratzoulas, S.; et al. Tuning the Reactivity of Carbon Surfaces with Oxygen-Containing Functional Groups. *Nat. Commun.* **2023**, *14*, 2293. [CrossRef]
34. Du, Y.-F.; Sun, G.-H.; Li, Y.; Cheng, J.-Y.; Chen, J.-P.; Song, G.; Kong, Q.-Q.; Xie, L.-J.; Chen, C.-M. Pre-Oxidation of Lignin Precursors for Hard Carbon Anode with Boosted Lithium-Ion Storage Capacity. *Carbon* **2021**, *178*, 243–255. [CrossRef]
35. Abimana, C.; Bello, A.; Machunda, R.; Chande Jande, Y.A. Understanding the Factors Influencing the Properties of Biomass-Derived Porous Carbon and Their Impacts on Electrical Double-Layer Capacitor Electrodes: A Comprehensive Review. *J. Renew. Energy* **2024**, *2024*, 1343256. [CrossRef]
36. Zuo, L.; Zhang, Y.; Zhang, L.; Miao, Y.-E.; Fan, W.; Liu, T. Polymer/Carbon-Based Hybrid Aerogels: Preparation, Properties and Applications. *Materials* **2015**, *8*, 6806–6848. [CrossRef]

37. Zhou, Z.; Liu, T.; Khan, A.U.; Liu, G. Controlling the Physical and Electrochemical Properties of Block Copolymer-Based Porous Carbon Fibers by Pyrolysis Temperature. *Mol. Syst. Des. Eng.* **2020**, *5*, 153–165. [CrossRef]
38. Bartoli, M.; Troiano, M.; Giudicianni, P.; Amato, D.; Giorcelli, M.; Solimene, R.; Tagliaferro, A. Effect of Heating Rate and Feedstock Nature on Electrical Conductivity of Biochar and Biochar-Based Composites. *Appl. Energy Combust. Sci.* **2022**, *12*, 100089. [CrossRef]
39. Melnikova, E.; Bogdanova, E.; Paveleva, D.; Saranov, I. Sucrose, Lactose, Thermogravimetry, and Differential Thermal Analysis: The Estimation of the Moisture Bond Types in Lactose-Containing Ingredients for Confectionery Products with Reduced Glycemic Index. *Int. J. Food Sci.* **2023**, *2023*, 8835418. [CrossRef]
40. Ferrero, C.; Martino, M.N.; Zaritzky, N.E. Effect of hydrocolloids on starch thermal transitions, as measured by DSC. *J. Therm. Anal.* **1996**, *47*, 1247–1266. [CrossRef]
41. Changmai, B.; Rano, R.; Vanlalveni, C.; Rokhum, S.L. A Novel Citrus Sinensis Peel Ash Coated Magnetic Nanoparticles as an Easily Recoverable Solid Catalyst for Biodiesel Production. *Fuel* **2021**, *286*, 119447. [CrossRef]
42. Muhammad, F.; Nisar, J.; Ali, G.; Anwar, F.; Wan Abdul Karim Ghani, W.A.; Sharif, A.; Ahmed, E. Pyrolysis of Sweet Lemon (*Citrus limetta*) Waste: Effect of Zeolite β, Ammonium on Kinetics and Bio-Oil Yield. *Energy Adv.* **2025**, *4*, 414–423. [CrossRef]
43. Sevilla, M.; Ferrero, G.A.; Fuertes, A.B. One-Pot Synthesis of Biomass-Based Hierarchical Porous Carbons with a Large Porosity Development. *Chem. Mater.* **2017**, *29*, 6900–6907. [CrossRef]
44. Xue, J.; Liu, D.; Li, D.; Hong, T.; Li, C.; Zhu, Z.; Sun, Y.; Gao, X.; Guo, L.; Shen, X.; et al. New Carbon Materials for Multifunctional Soft Electronics. *Adv. Mater.* **2025**, *37*, 2312596. [CrossRef] [PubMed]
45. Mohammadnabi, S.; Rahmani, K. Production and an Advanced Model for Electrical Conductivity of Silicone Rubber/Carbon Nanotube Nanocomposites as Outdoor Insulator Housing Material. *J. Compos. Mater.* **2023**, *57*, 3331–3345. [CrossRef]
46. Avilés, F. Thermoresistivity of Carbon Nanostructures and Their Polymeric Nanocomposites. *Adv. Mater. Interfaces* **2023**, *10*, 2300218. [CrossRef]
47. Kotsyubynsky, V.; Rachiy, B.; Boychuk, V.; Budzulyak, I.; Turovska, L.; Hodlevska, M. Correlation between Structural Properties and Electrical Conductivity of Porous Carbon Derived from Hemp Bast Fiber. *Fuller. Nanotub. Carbon Nanostruct.* **2022**, *30*, 873–882. [CrossRef]
48. Malkova, A.N.; Sipyagina, N.A.; Gozhikova, I.O.; Dobrovolsky, Y.A.; Konev, D.V.; Baranchikov, A.E.; Ivanova, O.S.; Ukshe, A.E.; Lermontov, S.A. Electrochemical Properties of Carbon Aerogel Electrodes: Dependence on Synthesis Temperature. *Molecules* **2019**, *24*, 3847. [CrossRef]
49. Gul, A.S.; Noman, M.; Rehman, Q.; Khan, A.D.; Rehan, M.S.; Jan, S.T.; Khan, A.D. Achieving Optimal Balance: Tuning Electrical and Optical Characteristics of Carbon Electrodes for Emerging Photovoltaics. *RSC Adv.* **2024**, *14*, 15571–15581. [CrossRef]

Disclaimer/Publisher's Note: The statements, opinions and data contained in all publications are solely those of the individual author(s) and contributor(s) and not of MDPI and/or the editor(s). MDPI and/or the editor(s) disclaim responsibility for any injury to people or property resulting from any ideas, methods, instructions or products referred to in the content.